JACS
JOURNAL OF THE AMERICAN CHEMICAL SOCIETY
pubs.acs.org/JACS
Article

Dicyanorhodanine-Pyrrole Conjugates for Visible Light-Driven Quantitative Photoswitching in Solution and the Solid State

Parag Das, Nathan J. Grinalds, Ion Ghiviriga, Khalil A. Abboud, Łukasz Dobrzycki, Jiangeng Xue,* and Ronald K. Castellano*

Cite This: https://doi.org/10.1021/jacs.4c00983
Read Online
ACCESS | Metrics & More | Article Recommendations | Supporting Information

ABSTRACT: Small molecule photoswitches capable of toggling between two distinct molecular states in response to light are versatile tools to monitor biological processes, control photochemistry, and design smart materials. In this work, six novel dicyanorhodanine-based pyrrole-containing photoswitches are reported. The molecular design avails both the *Z* and *E* isomers from synthesis, where each can be isolated using chromatographic techniques. Inter- and intramolecular hydrogen bonding (H-bonding) interactions available to the *E* and *Z* isomers, respectively, uniquely impart thermal stability to each isomer over long time periods. Photoisomerization could be assessed by solution NMR and UV−vis spectroscopic techniques along with complementary ground- and excited-state computational studies, which show good agreement. Quantitative $E \rightarrow Z$ isomerization occurs upon 523 nm irradiation of the parent compound (where R = H) in solution, whereas $Z \rightarrow E$ isomerization using 404 nm irradiation offers a photostationary state (PSS) ratio of 84/16 (E/Z). Extending the π-conjugation of the pyrrole unit (where R = p-C_6H_4−OMe) pushes the maximum absorption to the yellow-orange region of the visible spectrum and allows bidirectional quantitative isomerization with 404 and 595 nm excitation. Comparator molecules have been prepared to report how the presence or absence of H-bonding affects the photoswitching behavior. Finally, studies of the photoswitches in neat films and photoinactive polymer matrices reveal distinctive structural and optical properties of the *Z* and *E* isomers and ultimately afford reversible photoswitching to spectrally unique PSSs using visible light sources including the Sun.

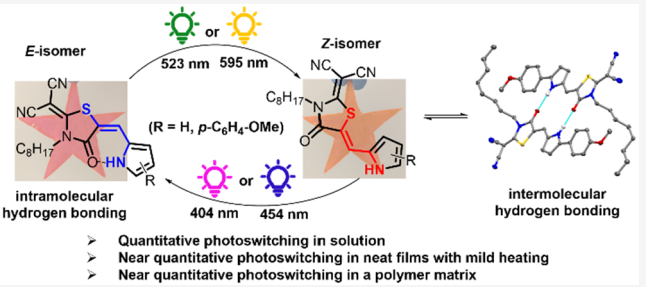

INTRODUCTION

Molecular photoswitches are a class of photochromic molecules that undergo reversible photochemical reactions using light as an external stimulus.[1] Two popular classes of photoswitching molecules include those that undergo reversible *Z*/*E* photoisomerization, azobenzene,[2] stilbene,[3] hemithioindigo[4] (HTI), and hydrazone,[5] and those that switch between open and closed forms through photoinduced reversible ring-opening/closing mechanisms such as spiropyran[6] and diarylethene.[7,8] Due to their ability to precisely control chemical and biological processes at the nanoscale,[9] these molecular photoswitches have received significant attention across many scientific disciplines and application areas including supramolecular chemistry,[10] material science,[11,12] molecular machines,[13] photopharmacology,[14] and drug delivery.[15] Considerable attempts have been made over the years to optimize molecular photoswitching behavior in terms of visible light switching,[16] isomer enrichment at the photostationary state (PSS),[17,18] reduced photodegradation or photoinduced side reactions,[19] and bidirectionally quantitative isomerization[20] through judicious structural modifications and complementary structure−property studies.[21]

Newhouse and coworkers reported bidirectionally quantitative HTI-photoswitches by utilizing electron-rich pyrroles that enable hydrogen bonding (H-bonding) interactions and lead to their superior switching properties (Figure 1a).[22] Dube and coworkers presented a survey of heterocyclic HTI-photoswitches that displayed notable photoswitching performances along with bistable isomers based on chalcogen and H-bonding interactions.[23] The same group recently reported aryl- and heteroaryl-based (e.g., imidazole, indole) rhodanine chromophores as highly photoswitchable motifs.[24]

2-(1,1-Dicyanomethylene)rhodanine, commonly known as dicyanorhodanine (RCN), is a popular electron acceptor unit in the organic photovoltaics (OPV) community.[25] Since its introduction in 2011, the RCN unit has served a significant role in the development of high-performing OPV materials in

Received: January 21, 2024
Revised: April 4, 2024
Accepted: April 5, 2024

https://doi.org/10.1021/jacs.4c00983
J. Am. Chem. Soc. XXXX, XXX, XXX−XXX

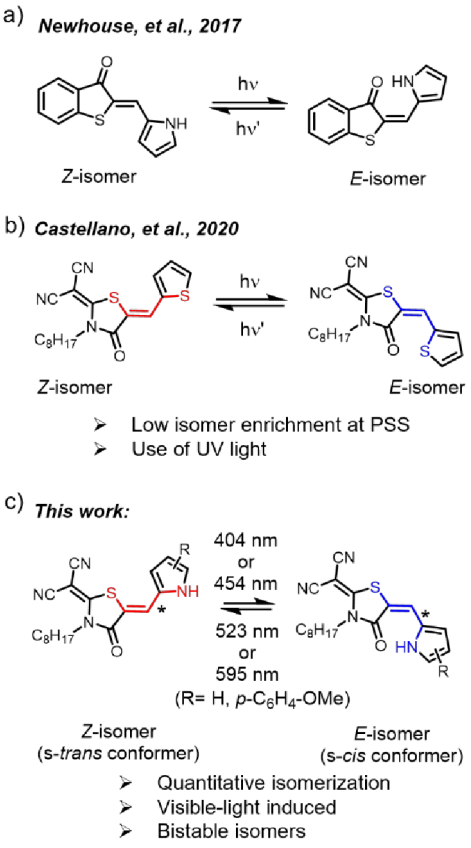

Figure 1. (a) Pyrrole-HTI photoswitches reported by Newhouse et al.[22] (b) *Z*/*E* photoisomerization of an RCN-functionalized thiophene conjugate.[27] (c) Visible light-induced quantitative *Z*/*E* photoisomerization of the RCN-functionalized pyrrole systems presented in this work. The molecules are depicted in the *Z* configuration (red) and the *E* configuration (blue). The conformation about the bond indicated with the asterisk (*) is shown as s-*trans* and s-*cis*, respectively, with respect to the nitrogen atom of the pyrrole unit.

acceptor−donor−acceptor (A-D-A) type small molecules.[26] Despite its popularity, the configurational and conformational complexity of RCN π-conjugated molecules have been largely neglected in the OPV literature. Our group recently brought attention to these features in a report on the *Z*/*E* photoisomerization behavior of RCN-functionalized oligothiophenes (Figure 1b) in solution[27] and the solid state.[28] In the latter work, *Z*/*E* configurational isomerization was shown to significantly affect thin-film morphology and optoelectronic properties.

Herein, we report the first RCN-pyrrole conjugates and their promising photoisomerization properties. Replacing the thiophene[27] unit with the H-bonding capable pyrrole unit (Figure 1c) secures red-shifted absorption profiles of both *Z* and *E* isomers relative to our previously reported compounds, thereby promoting visible light-induced quantitative isomerization. Intra- and intermolecular H-bonding available to the *E* and *Z* isomers, respectively, are hypothesized to be critical for photoswitch bistability and independent isomer isolation. By extending the π-conjugation on the pyrrole unit using electron-donating groups (EDGs), we have also realized bidirectional quantitative photoswitching in solution using alternating excitation of 404 and 595 nm. Photoswitching can also be performed in the solid state, both in a photoinactive polymer matrix and even neat films, where excellent reversibility is maintained in the former.

RESULTS AND DISCUSSION

Design and Synthesis. To evaluate the photoswitching capabilities of various pyrrole-containing RCN-functionalized compounds, we designed and synthesized six model chromophores (Figure 2). Compounds **1** and **2**, structural

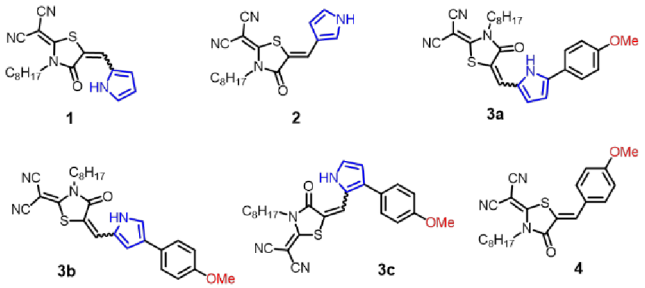

Figure 2. Chemical structures of RCN model compounds **1**−**4** studied in this work. As obtained from synthesis, compounds **1**, **3a**, **3b**, and **3c** are shown as mixtures of *Z* and *E* isomers, whereas compounds **2** and **4** are shown only in the *Z* configuration.

isomers, are the simplest RCN-pyrrole analogs and assess the influence of H-bonding on photoisomerization behavior. Structural isomers **3a**, **3b**, and **3c** feature extended π-conjugation by introducing a *p*-methoxybenzene group at the 5-, 4-, and 3-positions of the pyrrole unit, respectively. These compounds experience attractive, red-shifted absorbance and inform us how the regiochemistry of the electron-donating group affects molecular geometry, H-bonding strength, optoelectronic properties, and photoisomerization behavior. Compound **4** eliminates the H-bonding capability and allows the evaluation of photoswitching efficiency and synthetic accessibility when no H-bonding is present.

Full synthetic details are provided (Schemes S1−S6). Syntheses began with the preparation of the parent RCN acceptor unit (compound **5**, 1), followed by Knoevenagel

Scheme 1. Synthesis of Model Compounds 1-*Z* and 1-*E*

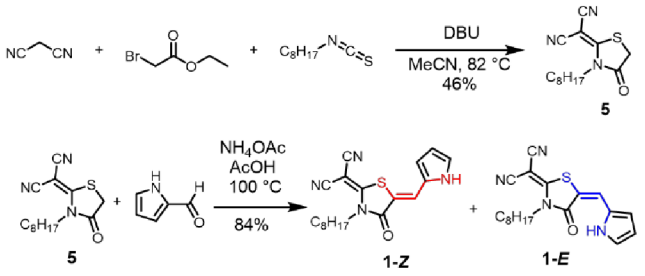

condensation with appropriate formylated heteroaryl/aryl units. For example, compound **1** was accessed through condensation between RCN (**5**) and pyrrole-2-carboxaldehyde which, interestingly, afforded both *Z* (69%) and *E* (31%) isomers (Scheme 1). Due to a large difference in polarity, as observed by thin-layer chromatography (TLC), the as-synthesized isomers could be separated using column chromatography (Figure S8). The ability to perform independent studies on pure *Z* and *E* isomers is a luxury not afforded by our previously studied RCN-oligothiophenes.[27]

https://doi.org/10.1021/jacs.4c00983
J. Am. Chem. Soc. XXXX, XXX, XXX−XXX

Structural Characterization of Parent Photoswitch 1. Compounds **1-*Z*** and **1-*E*** were characterized using ^{1}H NMR in chloroform-*d* (Figure S9). The —NH proton of the *E* isomer is more deshielded (δ = 12.35 ppm) than that of *Z* (δ = 8.96 ppm), a consequence of intramolecular H-bonding between the carbonyl oxygen of the RCN unit and the pyrrole —NH proton. Moreover, the olefin proton attached to the isomerizable C=C bond is more deshielded for the *Z* isomer (δ = 7.80 ppm) than for the *E* isomer (δ = 7.05 ppm), given its proximity to the electron-withdrawing carbonyl group of the RCN unit (Figure S9). Fourier-transform infrared (FT-IR) spectroscopy of compounds **1-*Z*** and **1-*E*** (5 mM, chloroform) confirmed that both the N—H and C=O stretching modes for the *E* isomer (3252 and 1688 cm^{-1}) are lower in wavenumber, broader, and higher in transmittance than those of the *Z* isomer (3456 and 1717 cm^{-1}), consistent with intramolecular H-bonding in the *E* isomer (Figure S13).

Solution Photoisomerization Behavior of Parent Photoswitch 1. We performed *Z*/*E* photoisomerization studies (15 mM, chloroform-*d*) of compound **1** with monitoring by ^{1}H NMR (details of irradiation sources can be found Figure S7). Quantitative *E* → *Z* photoisomerization was successfully obtained at 523 nm excitation (Figures 3a and S15, Tables 1 and S1). Upon selective excitation at 404 and 454 nm, *Z* → *E* photoisomerization was observed with a **1-*Z*/*E*** PSS ratio of 18/82 and 65/35, respectively (Figures 3b and S14, Tables 1 and S1).

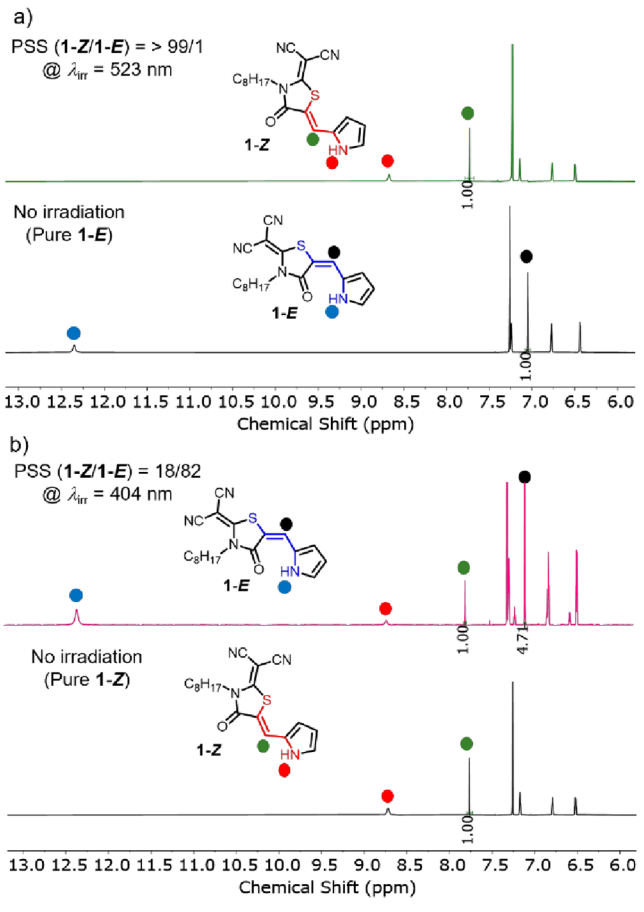

Figure 3. Solution ^{1}H NMR (15 mM, $CDCl_3$) photoisomerization studies of compound **1** showing (a) **1-*E*** → **1-*Z*** isomerization upon 523 nm excitation and (b) **1-*Z*** → **1-*E*** isomerization upon 404 nm excitation.

Next, we used UV−vis spectroscopy (20 μM, chloroform) to assess the photoisomerization behavior in-depth. The primary absorption peak maxima of **1-*Z*** and **1-*E*** were identified at 436 and 466 nm (Figures 4 and S24). The 30-nm wavelength difference in peak absorbance for **1-*Z*** and **1-*E*** (Table 1) is much larger than previously reported RCN-thiophene conjugates[27] and clearly influences the extent of photoisomerization. Gas phase time-dependent DFT (TD-DFT) calculations (CAM-B3LYP/cc-pVDZ) predict a 24-nm wavelength difference in peak absorption between **1-*Z*** and **1-*E*** with absorption maxima at 353 and 377 nm, in good agreement with experimental values (Figures 4 and S24). Performing the TD-DFT calculations using a solvent model (IEFPCM, chloroform) at the same level of theory, a very similar trend in the *Z* and *E* isomer absorption profiles, was observed (Figure S90). However, red-shifted absorption maxima were observed for both **1-*Z*** (λ_{max} = 378 nm) and **1-*E*** (λ_{max} = 397 nm), which can be attributed to the different dielectric properties offered by the solvent (chloroform).[29] The primary absorption bands of the model compounds are attributed to the HOMO−LUMO transitions, as confirmed by inspection of the frontier molecular orbitals through DFT simulations (Figure S76, Tables S6−S9). The *Z*/*E* photoisomerization behavior observed for **1-*Z*** and **1-*E*** using UV−vis spectroscopy (Figure S30) is consistent with the isomerization behavior observed by NMR. A photoswitching experiment was performed using alternating 404 and 523 nm irradiation to promote *Z* → *E* and *E* → *Z* photoisomerization, respectively. Facile photoswitching is observed even after ten cycles, indicating the system is highly fatigue resistant (Figure S37).

Solution Photoisomerization Studies of Comparator 2. Comparator molecule **2** was detected only in the *Z* configuration from synthesis, unlike molecule **1**, since changing the connectivity between the RCN and pyrrole units removes the intramolecular H-bonding that stabilizes the *E* configuration. Furthermore, 254 and 404 nm irradiations result in **2-*Z*/2-*E*** mixtures with PSS ratios of 67/33 and 58/42, respectively (Figure S16, Tables 1 and S1). TD-DFT studies reveal a significant overlap of the **2-*Z*** and **2-*E*** absorption profiles (Figure S25), which rationalizes the incomplete *Z* → *E* photoisomerization observed with UV−vis spectroscopy (Figure S31). TLC of a **2-*Z*/2-*E*** mixture demonstrates that the **2-*E*** isomer has a minimal difference in the R_f value from **2-*Z*** (Figure S8), and these isomers could not be separated. These findings demonstrate the importance of H-bonding to the superior photoisomerization and synthetic accessibility of compound **1** over compound **2**.

Structural Characterization of π-Extended RCN-Pyrrole Conjugates. The photoswitching performance of pyrrole-RCN conjugates with greater π-conjugation was explored using compounds **3a**−**3c**. For all three versions of compound **3**, both *Z* and *E* isomers were identified from synthesis and could be isolated using column chromatography (Figure S8), like compound **1**. The isomers were distinguished following the same trend in chemical shifts from ^{1}H NMR spectroscopy

observed for compound **1**. For compound **3a** (Figure S10), the —NH proton peak is found to be more shielded for the *Z* isomer (δ = 9.06 ppm) compared to *E* (δ = 12.91 ppm), which again supports intramolecular H-bonding in the *E* isomer. The *Z* and *E* isomers of compounds **3b** (Figure S11) and **3c**

https://doi.org/10.1021/jacs.4c00983
J. Am. Chem. Soc. XXXX, XXX, XXX−XXX

Table 1. DFT-Simulated and Solution Absorption and Photoisomerization Studies of Model Compounds 1−4

	gas phase DFT studies				solution studies in chloroform				
	relative energy (kcal/mol)[a]		absorption maximum (nm)		absorption maximum (nm)		$\Delta\lambda_{abs}$ (nm)	Z/E composition (%/%) at the PSS[b]	
model compounds	Z	E	Z	E	Z	E	$\Delta_{E/Z}$	Z→E (λ_{irr} in nm)	E→Z (λ_{irr} in nm)
1	3.68	0	353	377	436	466	30	18/82 (404)	>99/1[c] (523)
2	0	2.57	329	350	407	N/A[d]	N/A[d]	58/42 (404)	N/A[d]
3a	4.10	0	393	432	492	534	42	<1/99[c] (404, 454)	>99/1[c] (595)
3b	3.61	0	371	399	462	493	31	24/76 (454)	>99/1[c] (523)
3c	4.02	0	375	398	458	488	30	17/83 (404)	>99/1[c] (523)
4	0	4.17	344	360	411	N/A[d]	N/A[d]	53/47 (404)	N/A[d]

[a]Energy values reported of the most stable conformer in the Z and iE states [b]For each sample, the PSS ratios have been reported based on three measurements (with an error of ±1%). [c]Quantitative photoisomerization observed. [d]The pure E isomer could not be isolated to perform independent solution studies.

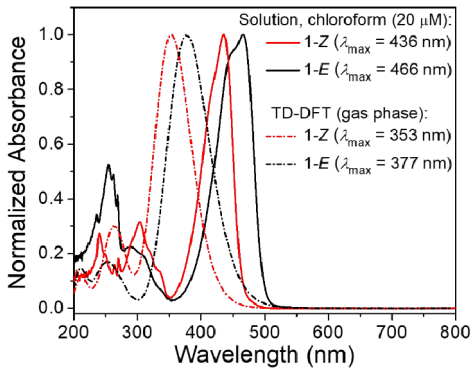

Figure 4. Solution (solid lines) UV−vis (20 μM, chloroform) and gas phase TD-DFT-predicted (dashed lines) absorption profiles of compounds **1-*Z*** (red spectra) and **1-*E*** (black spectra).

(Figure S12) show similar chemical shift trends. Stereochemical analysis was conducted using 2D NMR experiments (Figures S1−S6), including in-phase/antiphase gradient-selected heteronuclear single- and multiple-bond correlation (IPAP-gHSMBC) spectroscopy. 2D NMR analysis (Figure S6) of a **3b-*Z*/3b-*E*** mixture (chloroform-*d*) obtained via irradiation to the PSS (using 454 nm LED) indicates the three-bond heteronuclear coupling ($^{1,3}J$) between the rhodanine C═O, and the isomerizable olefin is larger for the *E* isomer ($^{1,3}J_{C3-H8}$ = 11 Hz) compared to the *Z* ($^{1,3}J_{C3-H8}$ = 5.7 Hz), which is in compliance with our previous RCN work.[27]

We were also able to obtain the single-crystal X-ray structures of compounds **3a-*Z*** (Figure 5) and **3b-*Z*** (Figures S91−S100, Tables S12−S14). The Oak Ridge Thermal Ellipsoid Plot (ORTEP) of **3a-*Z*** confirms the *Z* stereochemistry of the molecule about the exocyclic olefin. A twisted geometry is adopted by **3a-*Z*** in the crystal, likely to minimize the steric interactions with deviations from planarity. This is defined by the dihedral angles S1−C14−C24−C25 (−5.44°) and N1−C7−C1−C6 (−16.27°, Figure 5b). The unit cell contains two molecules (Z = 2) of **3a-*Z*** (Figure 5c), and the $\pi-\pi$ distance between the two monomers is found to be 3.38 Å, as measured between planes defined by the cyclic RCN (Figure 5c). One *Z* monomer can participate in intermolecular H-bonding through the carbonyl oxygen (O_2) of the RCN unit, with the hydrogen attached to the pyrrole nitrogen (N1) of another monomer to form a dimeric structure. The distance between the hydrogen and the carbonyl oxygen is found to be 2.16 Å (Figure 5d). The long-range packing of **3a-*Z*** displays a cofacial, head-to-tail arrangement (Figure 5e). Compound **3b-**

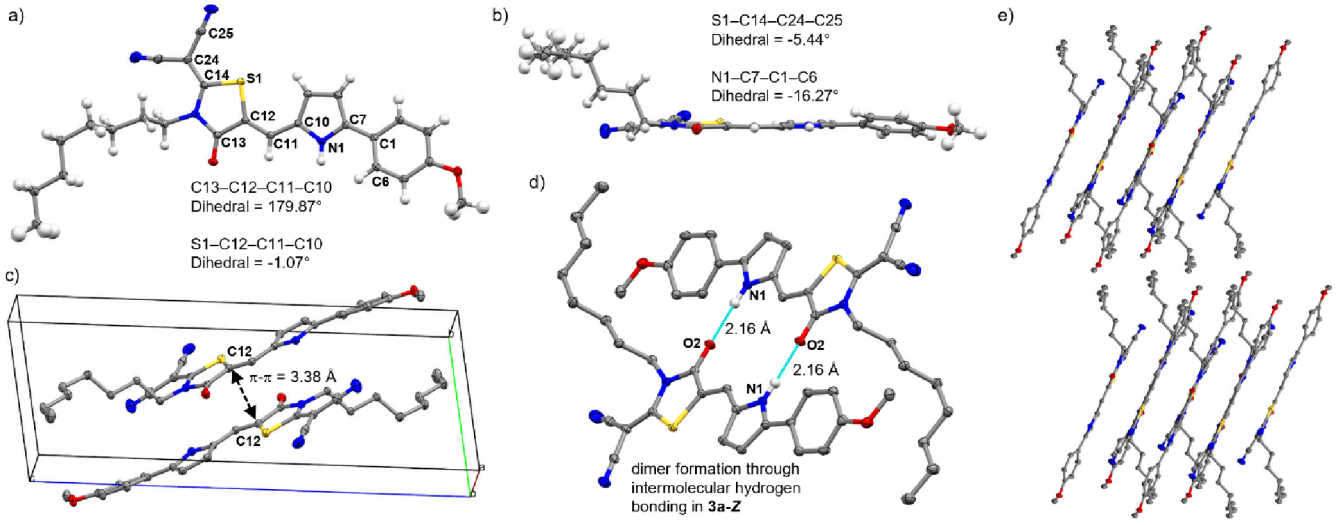

Figure 5. Single-crystal X-ray analysis of **3a-*Z***. (a) ORTEP representation of the **3a-*Z*** monomer, face-on view (thermal ellipsoids are set at a 50% probability level). (b) Edge-on view of the **3a-*Z*** monomer. (c) Unit cell containing two molecules of **3a-*Z***. (d) Dimeric interaction through intermolecular hydrogen bonding between two monomers of **3a-*Z***. (e) Long-range packing of **3a-*Z*** in the solid state (view along 100 plane).

https://doi.org/10.1021/jacs.4c00983
J. Am. Chem. Soc. XXXX, XXX, XXX−XXX

Z also adopts a twisted geometry in the crystalline state, defined by the dihedrals S1−C14−C24−C25 (4.82°) and C7−C8−C1−C2 (23.21°, Figure S94), indicating that the **3b-Z** regiochemistry forces a slightly more twisted structure than **3a-Z**. The unit cell comprises eight monomers ($Z = 8$) of **3b-Z** (Figure S95a), and the presence of the intermolecular H-bonded dimer is observed, like **3a-Z**, with an H-bonding distance of ∼2 Å (Figure S95b). Interestingly, the **3b-Z** crystals undergo reversible phase transition in the range of 290 K−300 K on heating (Figures S99 and S100, Table S14). The high-temperature polymorph measured at 300 K was found to be disordered with four monomers in the unit cell ($Z = 4$).

Enhanced Photoswitching Behavior of 3a−3c. ^{1}H NMR was used to monitor the photoswitching of the three versions of compound **3** using various excitation sources (Table 1 and Figures S17−S22). For compound **3a** (15 mM, chloroform-*d*), quantitative $E \rightarrow Z$ photoisomerization was achieved using 595 nm irradiation (Figure 6a), while 404 and

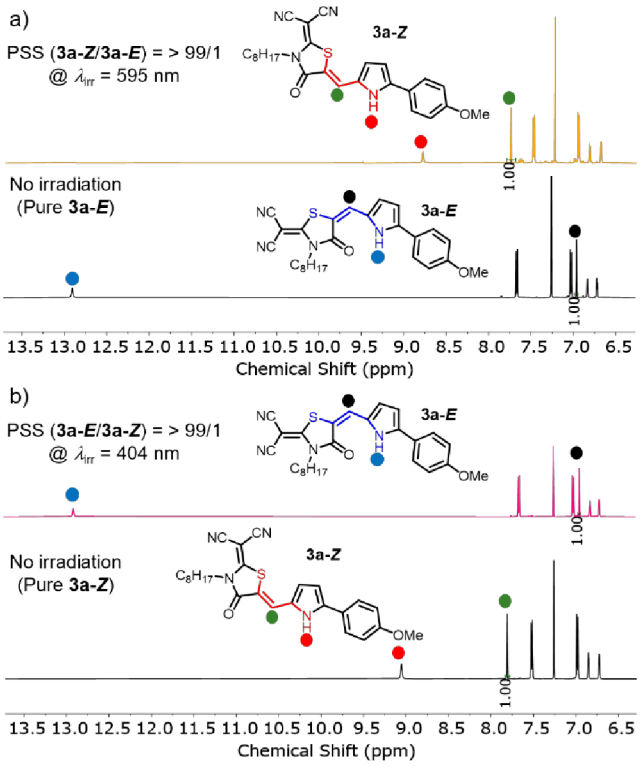

Figure 6. Solution ^{1}H NMR (15 mM, $CDCl_3$) photoisomerization studies of compound **3a** showing (a) **3a-*E*** → **3a-*Z*** isomerization upon 404 nm excitation. (b) **3a-*Z*** → **3a-*E*** isomerization upon 595 nm excitation.

454 nm irradiation revealed quantitative $Z \rightarrow E$ switching (Figure 6b), indicating complete bidirectional photoswitching. Quantitative $E \rightarrow Z$ photoisomerization was also achieved when **3b-*E*** and **3c-*E*** were irradiated at 523 nm. Excitation of **3b-*Z*** and **3c-*Z*** at 404 or 454 nm, while not quantitative, leads to PSSs composed of ∼80% *E*. Achieving quantitative bidirectional photoswitching with compounds **3b** and **3c** might be possible with the correct choice of solvent and excitation wavelength, which warrants further investigation.

The UV−vis absorption spectra of compound **3a** displays a large red shift for both *Z* and *E* isomers in solution relative to compound **1** with absorption maxima at 492 and 534 nm, respectively (Figure 7a). The 42 nm difference in maximum absorption between *E* and *Z* isomers explains the well-behaved

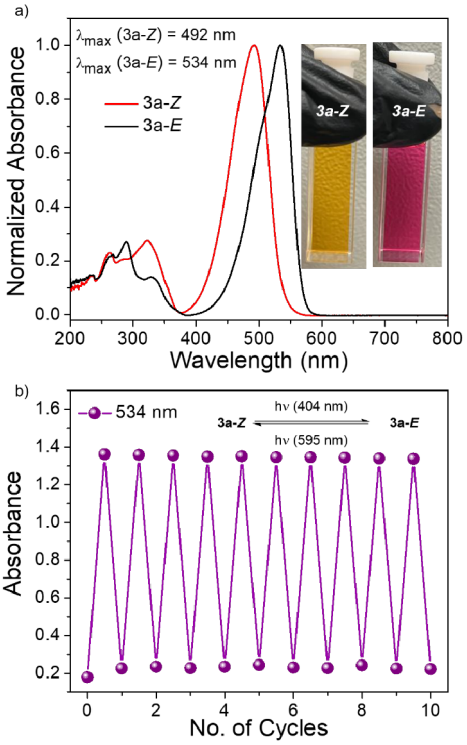

Figure 7. (a) Solution UV−vis (20 μM, chloroform) spectra of compounds **3a-*Z*** (red spectrum) and **3a-*E*** (black spectrum), inset: as-prepared solutions of **3a-*Z*** and **3a-*E*** in a 1-cm quartz cuvette. (b) UV−vis photoswitching of compound **3a** (20 μM, chloroform). The absorbance change at 534 nm was monitored while alternating between 404 and 595 nm irradiation.

bidirectional quantitative switching behavior of **3a**. The large difference in peak absorbance wavelength between the **3a** isomers is well-supported by TD-DFT (Figure S26). The pronounced difference in color (Figure 7a, inset) of compounds **3a-*Z*** (yellow-orange) and **3a-*E*** (red-violet), along with excellent photochromism, is quite interesting in terms of their potential solid-state applications as sensors or smart materials.[30]

Compared with **3a**, compounds **3b** and **3c** show hypsochromic shifts for both *Z* and *E* isomers. Absorption maxima of **3b-*Z*** and **3b-*E*** are found at 462 and 493 nm, respectively, whereas for **3c-*Z*** and **3c-*E***, the peaks lie at 458 and 488 nm, respectively (Figures S27−S28). The absorption spectra for compounds **3a−3c** (Figures S26−S28) determined by using TD-DFT simulations agree well with the trends observed in solution. The higher-energy absorption maxima of **3b** and **3c** compared to **3a** suggest the extent of π-electron delocalization is significantly less with arylation at the 3- and 4-positions of the pyrrole compared to the 5-position.[31]

Z/*E* photoisomerization studies of series **3** in solution (20 μM, chloroform) using UV−vis (Figures S32−S34) are consistent with the photoisomerization behavior observed using NMR. Bidirectional complete photoisomerization is achieved for compound **3a**, and a photoswitching experiment could be performed using alternating 404 and 595 nm irradiation to promote $Z \rightarrow E$ and $E \rightarrow Z$ photoisomerization, respectively. The system appears to be highly fatigue resistant

https://doi.org/10.1021/jacs.4c00983
J. Am. Chem. Soc. XXXX, XXX, XXX−XXX

after ten cycles (Figures 6b and S37). Facile photoswitching is also observed for compounds **3b** (Figure S38) and 3c (Figure S39), highlighting the excellent switching behavior of these compounds. Photoluminescence studies in solution (20 μM, chloroform) of two model compounds, **3a** and **3b**, were also performed. Both the *Z* and *E* isomers exhibit considerable luminescence when excited at their respective absorption maxima. For compound **3a**, the emission maxima of the *Z* and *E* isomers are observed at 570 and 572 nm, respectively. For compound **3b**, the emission maxima of the *Z* and *E* isomers are found at 553 and 570 nm, respectively (Figure S41). The photoluminescence of the RCN-pyrrole conjugates is promising for the design of emissive photoswitches upon further molecular engineering in the future.[32]

To assess the overall efficacy of pyrrole (and arylated pyrrole) units on the photoswitching properties of RCN molecules, comparator molecule **4** was synthesized through condensation of RCN and *p*-methoxybenzaldehyde. Only the *Z* isomer was obtained from the synthesis. As determined by ^{1}H NMR, 254 and 404 nm irradiation results in a **4-*Z*/4-*E*** mixture with a PSS ratio of 71/29 and 53/47 (Figure S23, Tables 1 and S1). Both solution (20 μM, chloroform) and TD-DFT studies show lower-wavelength absorption maxima for **4-*Z*** at 411 and 344 nm, respectively, (Figure S29) compared to the RCN-pyrrole switches. UV−vis spectroscopy reports incomplete *Z* → *E* photoisomerization in solution for compound **4** (Figure S35), providing further evidence that pyrrole-conjugated RCN molecules are more efficient photoswitches.

Origins of Bistability. For most of the common photoswitching molecules such as azobenzenes and HTIs, one of the isomers is more thermodynamically stable. Consequently, only one isomer is available from synthesis, while the other metastable isomer is obtainable by photoirradiation. Surprisingly, both *Z* and *E* isomers were accessible from synthesis for RCN-pyrrole switches **1** and **3a**−**3c**. These observations were repeatable even with the reaction vessels being covered with aluminum foil throughout the entire synthesis and purification processes to minimize the possibility of unintentional photoisomerization by ambient light. This unique isomer accessibility from synthesis is dissimilar to our previous work on RCN[27] and INCN-functionalized[33] thiophene oligomers, where only the more thermodynamically stable *Z* isomer could be obtained from synthesis.

We speculate that the intermolecular H-bonding in the *Z* isomers and intramolecular H-bonding in the *E* isomers facilitate two thermodynamically stable states. While the intramolecular H-bond interaction between the carbonyl oxygen and pyrrole —NH in the *E* isomer is obvious as confirmed by NMR and IR spectroscopic techniques (Figures S9 and S13), the intermolecular H-bonding in the *Z* isomer is demonstrated by the crystal structures of **3a-*Z*** and **3b-*Z***. As shown in Figures 5d and S95b, *Z* monomers can participate in intermolecular H-bonding to form dimeric structures. The extent to which H-bonding enhances the stability of both isomers is described below.

To gain more insight into the origin of bistability, we performed gas phase DFT calculations (B3LYP/6−31+G(d)) to compare the molecular structures of the *E* and *Z* isomers. For compound **1**, a planar geometry was obtained for both **1-*Z*** and **1-*E*** (Figure 8a,b). However, when the relative energies of the isomers were compared, the s-*cis* conformer of **1-*E*** was most stable, while the s-*trans* conformer of **1-*Z*** was 3.68 kcal/mol higher in energy (Table 1). The intramolecular H-bonding interaction between the —NH proton and carbonyl oxygen in the *E* isomer (Figure 8a), characterized by an O···H distance of 1.83 Å and C═O···H angle of 117°, has been discussed in related contexts.[22] Solvent model calculations (IEFPCM, chloroform) also present the **1-*E*** isomer as thermodynamically more stable than **1-*Z*** (by 1.89 kcal/mol), possibly due to the presence of intramolecular H-bonding in the *E* form (Figure S89). The difference observed in the relative stability of the two isomers from the gas phase and the solvent model DFT calculations can be attributed to the change in the interfacial and dielectric properties offered by the solvent versus the in-vacuum conditions for the gas phase calculations.

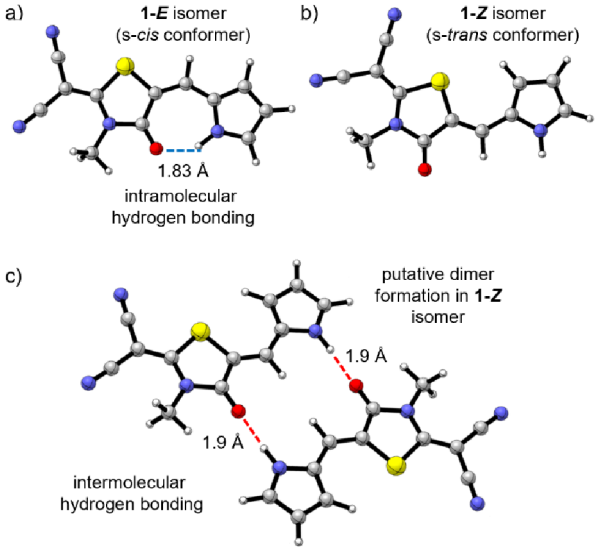

Figure 8. Optimized lowest energy conformers (DFT, B3LYP/6−31+G(d)) of (a) **1-*E*** (face-on view, showing possible intramolecular hydrogen bonding interaction) and (b) **1-*Z*** (face-on view). (c) Putative dimer formation of **1-*Z*** through intermolecular hydrogen bonding interactions.

As the stability of the *Z* isomer can come in part from self-association, first observed by X-ray analysis, we also found that the DFT calculations support the geometric requirements for this interaction quite well. A putative **1-*Z*** dimer would form through two H-bonds, with O···H distances of 1.9 Å and a C═O···H angle of 179°, which is typical for intermolecular H-bonding (Figure 8c).[34] The gas phase-binding enthalpy of the dimer, −13.63 kcal/mol (−6.82 kcal/mol per **1-*Z*** monomer) could explain the stability of the *Z* isomer if preserved in solution.[35] Similar dimeric interactions through intermolecular H-bonding were previously reported in related conjugated molecules.[34,36] When considering the monomeric state for compounds **3a**−**3c**, the *E* isomer was found to be more stable than *Z* due to the presence of intramolecular H-bonding in the s-*cis* conformer of the *E* state (Table 1). However, for comparators **2** and **4**, the *Z* isomer is found to be more stable than the *E* isomer, which is consistent with observations during synthesis (Table 1). Computational details of all compounds are available (pages S81−S107).

Assessment of H-Bonding Interactions. To deepen our understanding of the H-bonding interactions present in the *Z* and *E* isomers, temperature-dependent ^{1}H NMR was performed from 25 to 90 °C (15 mM, tetrachloroethane-d_2). For compound **1-*Z***, a gradual upfield chemical shift (8.86 to 8.68 ppm, $\Delta\delta$ = 0.18 ppm) of the —NH proton was observed

https://doi.org/10.1021/jacs.4c00983
J. Am. Chem. Soc. XXXX, XXX, XXX−XXX

when increasing the temperature from 25 to 90 °C (Figure S57). Upon gradual cooling of the sample back to 25 °C, a downfield chemical shift (8.68 to 8.85 ppm, $\Delta\delta$ = 0.17 ppm) was observed (Figure S58). This suggests that the intermolecular H-bonding might be disrupted as the temperature increases, breaking the dimeric interactions present in **1**-*Z*. Similar experiments with compound **1**-*E* demonstrated only a very small shielding (12.32 ppm to 12.29 ppm, $\Delta\delta$ = 0.03 ppm) and deshielding (12.29 ppm to 12.32 ppm, $\Delta\delta$ = 0.03 ppm) of the —NH proton peak upon increasing and decreasing the temperature (Figures S59−S60). For compound **2**-*Z* (Figures S61−S62), the change in chemical shift of the —NH proton was found to be 0.09 ppm, around half of the change found in the case of **1**-*Z*. These results further justify that the —NH proton in **1**-*Z* is involved in intermolecular H-bonding, in contrast to the temperature insensitive -NH proton in **1**-*E* that is engaged in intramolecular H-bonding (Figure S63). Similar studies (15 mM, tetrachloroethane-d_2) with compounds **3a**-*Z* ($\Delta\delta$ = 0.22 ppm, Figure S64) and **3b**-*Z* ($\Delta\delta$ = 0.18 ppm, Figure S65) also show shielding of the —NH proton peak upon gradual increase of temperature from 25 to 90 °C, consistent with the disruption of dimerization at higher temperatures.

We also performed concentration-dependent studies for compound **1**-*Z* (chloroform-*d*) from 2 to 30 mM. A downfield shift (8.64 to 8.71 ppm, $\Delta\delta$ = 0.07 ppm) of the —NH proton peak is observed with increasing concentration, which also points to H-bonding present in the *Z* isomer (Figure S66). However, for compound **3a**-*Z* (1 mM to 50 mM, chloroform-*d*), a significantly larger downfield chemical shift change ($\Delta\delta$ = 0.81 ppm) is observed upon increasing the concentration (Figure S67), which suggests that the electronics of these RCN-pyrrole conjugates influence the strength of dimeric association.

Thermal Isomerization Studies. Remarkably, no thermal isomerization was observed in either direction for **1**-*Z* and **1**-*E* in tetrachloroethane up to 80 °C (Figures S68−S69) or in acetonitrile-d_3 up to 60 °C (Figures S70−S71) over 120 and 80 h, respectively, which speaks to the bistable nature of the isomers. These findings deviate from our previous work on INCN-based donor−acceptor molecules, where we observed that higher polarity solvent induced faster thermal isomerization compared to a lower polarity solvent, in case of an INCN-monothiophene analog.[33] In a H-bonding competitive solvent such as DMSO-d_6 at 60 °C, no *Z* → *E* thermal isomerization was observed within 80 h (Figure S72), but the 1-*E* isomer relaxes to **1**-*Z* completely within 3 h (Figure S73). In DMSO, the *Z* isomer is preferred because DMSO can stabilize the *Z* isomer through intermolecular H-bonding (Figures S72−S73). The thermal half-life of the **1**-*E* isomer is calculated as 3.18 h in DMSO at 298 K (pages S78−S80). These studies reveal that the thermodynamic preference of the *Z* and *E* isomers is highly solvent dependent and worthy to explore in a wide range of solvents in the future.

The thermal stability of both isomers of compound 1 was also evidenced during the thermal gradient sublimation studies. Both **1**-*Z* and **1**-*E* were obtained in pure forms after being subjected to temperatures over 130 °C at <1 × 10^6 Torr for 24−72 h (Figures S55−S56). This suggests that, in addition to solution processing, these materials could be vacuum deposited, which is advantageous for the fabrication of certain electronic devices like thin-film transistors or in situations where interactions with solvent are undesirable.

Optoelectronic Studies of Thin Films. The optoelectronic properties of compounds **1** and **3a** were also investigated in the solid state to explore if their well-behaved photoswitching could be extended to environments more suitable for applications in photoresponsive materials,[11] optoelectronics,[37] and photonic computing.[38] The UV−vis absorption and photoluminescence (PL) data were obtained for neat films fabricated via spin coating, which were characterized as-spun and after thermally annealing at 80 °C for 15 min (Figure 9). The absorption and PL of the **1**-*Z* films

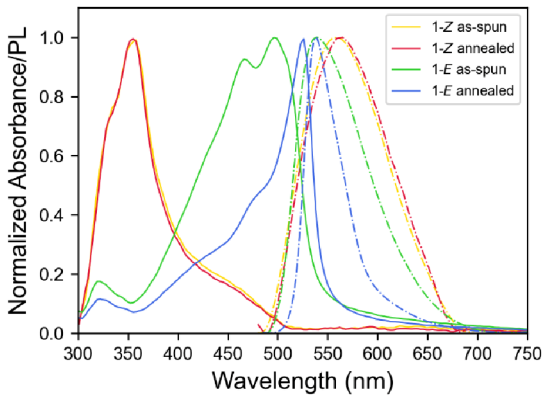

Figure 9. Normalized UV−vis absorption (solid lines) and normalized photoluminescence (PL, dashed lines) spectra for neat films of compounds **1**-*Z* and **1**-*E*.

is consistent with the formation of H-aggregates evidenced by the significant reduction in oscillator strength for the $\pi \rightarrow \pi^*$ transition around 440 nm relative to its solution absorption, very weak PL emission, and large Stokes shift (~135 nm).[39] The **1**-*Z* films display well-ordered packing following the spin-coating process, with no noticeable changes in absorption after annealing. In contrast, the **1**-*E* films display absorption and PL spectra consistent with J-aggregation evidenced by absorption that is 30 nm red-shifted relative to its solution absorption for as-spun films and 60 nm red-shifted for thermally annealed films. Thermal annealing enhances the PL intensity 3-fold for **1**-*E* films with a Stokes shift of just 7 nm, which is characteristic of J-aggregates,[40] and suggests that as-spun films are relatively amorphous, but more crystalline domains form upon annealing.

The tendency of *Z* isomers to form H-aggregates and *E* isomers to form J-aggregates was also observed for **3a** thin films (Figure 10). After spin coating, as-spun **3a**-*Z* films display absorption spectra reminiscent of their solution absorption, indicating the films are primarily amorphous. After thermal annealing, the $\pi \rightarrow \pi^*$ transition decreases significantly and is accompanied by a new blue-shifted peak at 388 nm due to H-band absorption. Further evidence for the formation of H-aggregates in the case of **3a**-*Z* comes from single-crystal X-ray diffraction (see Figure 5), which illustrates the typical cofacial molecular stacking with a slip angle (i.e., the angle between the stacking axis and the long molecular axis) of about 73°.

Like the **1**-*E* films, the **3a**-*E* films appear amorphous after spin coating and become well-ordered J-aggregates after thermal annealing with the lowest energy peak for as-spun films 13 nm red-shifted relative to the solution absorbance and 31 nm red-shifted for annealed films. The **3a**-*E* PL intensity increases 10-fold after annealing and the fwhm narrows from 0.30 to 0.15 eV indicating a reduction in the static energetic

https://doi.org/10.1021/jacs.4c00983
J. Am. Chem. Soc. XXXX, XXX, XXX−XXX

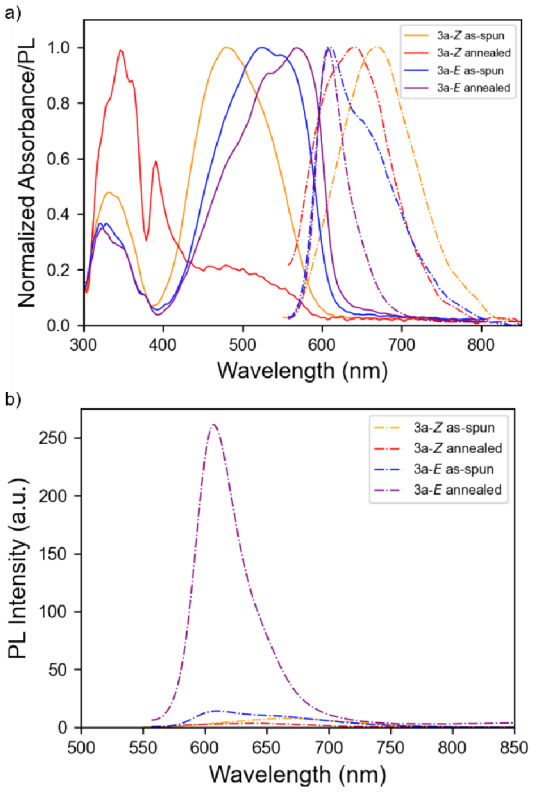

Figure 10. (a) Normalized UV−vis absorption (solid lines) and normalized photoluminescence (PL, dashed lines) spectra for films of compounds **3a-*Z*** and **3a-*E***. (b) Raw PL intensity for the same films when excited at 495 nm.

disorder present in the films[41] and crystallization-induced emission enhancement (CIEE).[42] The synergy of planarity and J-aggregation in the solid-state is known to be propitious for achieving aggregation-induced emission enhancement (AIEE),[43] which is intrinsic to the *E* isomer for compounds **1** and **3a** and is favorable for developing luminescent organic materials.

The annealed **3a-*E*** films display a 42 nm Stokes shift compared to ∼160 nm for annealed **3a-*Z*** films. The remarkable differences in aggregation behavior and optical properties between the *E* and *Z* isomers in neat films of **1** and **3a** motivated photoswitching studies of their neat films in the hope of reversibly achieving these distinctive states. These distinct features of isomer-specific J- and H-aggregation for the RCN-pyrrole molecules are quite unique and desirable.[44]

Photoisomerization Experiments on Neat Films. Neat as-spun films of compound **1-*E*** that were irradiated at 454 nm at room temperature only displayed minor $E \rightarrow Z$ conversion after 1 h of irradiation (Figure S45). However, when the as-spun 1-*E* films were simultaneously heated at 55 °C and irradiated at 454 nm, the $E \rightarrow Z$ conversion was almost complete after 1 h (Figure S46). For annealed **1-*E*** films, no $E \rightarrow Z$ conversion was observed at room temperature or while heated to 55 °C under 454 nm irradiation over 1 h (Figures S45−S46). From these data, it is evident that the as-spun **1-*E*** films have sufficient motional degrees of freedom to photoisomerize at room temperature (and more so if gently heated), while the tight molecular packing in the annealed **1-*E*** films resists isomerization even when heated. Interestingly, photoswitching studies of as-spun and annealed **1-*Z*** films showed that 404 nm light could be used to promote $Z \rightarrow E$ photoisomerization (Figures S47−S48). The attempt to fully reverse back to the pure *Z* state with 523 nm light was unsuccessful, although different light sources may enable this capability. We speculate that the tendency of **1-*Z*** thin films to undergo photoisomerization to a greater extent than **1-*E*** films is due to their aggregation mode (H versus J) and the strength of π-stacking.

In addition to compound **1-*Z***, as-spun **3a-*Z*** thin films displayed significant $Z \rightarrow E$ photoisomerization over 60 min with 454 nm irradiation at room temperature (Figure 11). Compounds **1** and **3a** are the first compounds for which we have observed $Z \rightarrow E$ photoisomerization in neat films among our synthesized RCN-functionalized compounds.

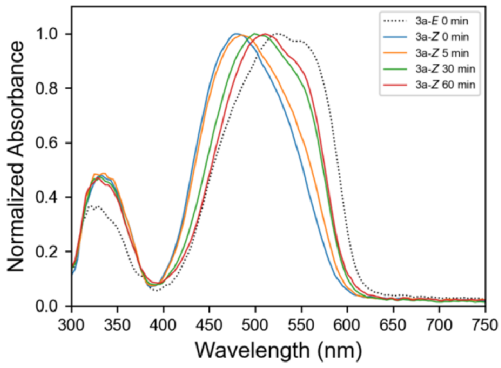

Figure 11. UV−vis absorption spectra for neat as-spun **3a-*Z*** films after prolonged intervals of 454 nm irradiation.

Surprisingly, $Z \rightarrow E$ photoisomerization was also observed in annealed **3a-*Z*** films, although to a lesser extent (Figure S51). When the sample is simultaneously heated at 55 °C and irradiated at 454 nm, the $Z \rightarrow E$ conversion is accelerated significantly (Figure S52). We attribute the capability of **3a-*Z*** to isomerize to the *E* state, even after its films have been thermally annealed, to its nonplanar structure, which reduces the strength of its $\pi-\pi$ interactions and provides more space to isomerize. Once the **3a** molecules reach the *E* state, the intramolecular H-bonding promotes a planar structure with stronger $\pi-\pi$ interactions, which resists conversion back to the *Z* state. Indeed, almost no $E \rightarrow Z$ photoisomerization was observed for as-spun or annealed **3a-*E*** films under 595 nm irradiation, even with heating to 55 °C (Figures S49−S50).

Photoswitching Experiments in a Polymer Matrix. Because intermolecular interactions prohibited the reversible photoisomerization of compounds **1** and **3a** in neat films, their photoswitching behavior was explored in a photoinactive polymer matrix to disrupt their aggregation. Polystyrene films were loaded with 1 wt % (w/w) of compounds **1** and **3a** prepared via spin coating from 80 mg/mL polystyrene solutions in chloroform. To our excitement, reversible photoswitching to two unique photostationary states was observed for both compounds, regardless if they were initially loaded with *E* or *Z* isomers. The **1-*E*** PSS after 523 nm irradiation is consistent with near-quantitative conversion to **1-*Z***, while the 404 nm PSS shows conversion back to an *E*-enriched state, although not complete (Figure S53). The same PSSs were achieved after another cycle of irradiation, showing that the conversion was reversible (Figure S53).

The polystyrene films doped with **3a-*Z*** reached a heavily *E*-enriched PSS under 404 nm irradiation, and a *Z*-enriched PSS

https://doi.org/10.1021/jacs.4c00983
J. Am. Chem. Soc. XXXX, XXX, XXX−XXX

under 595 nm irradiation (Figure 12). The same PSSs were achieved after another cycle of irradiation, showing that the

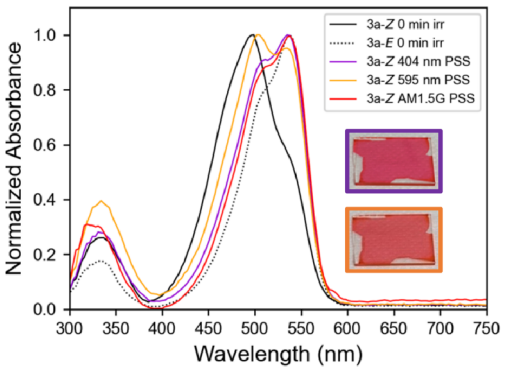

Figure 12. UV−vis absorption spectra for polystyrene films loaded with 1 wt % (w/w) **3a-*Z*** and **3a-*E*** and the photostationary states for films containing **3a-*Z*** after 45 min of irradiation at 404 and 595 nm or 10 min under 1 sun intensity (AM1.5G). Picture insets show images of **3a-*Z*** films at 404 nm PSS (violet) and 595 nm PSS (orange).

conversion was reversible (Figure S54). The polystyrene: **3a-*Z*** films were also irradiated under the AM1.5G spectrum by using a solar simulator to test if sunlight could be used to induce photoswitching. The AM1.5G PSS closely matches the *E*-enriched 595 nm PSS, which indicates that photoswitching from *Z* to *E* can be carried out by simply going outside for a few minutes (Figure 12).

While performing the photoswitching studies of compounds **1**−**3**, either in solution or in the solid-state, we have only observed facile well-controlled isomerization. Hence, we do not suspect a competing excited-state intramolecular proton transfer (ESIPT) mechanism,[45] although this has been observed in HTI-derived photoswitches limiting their isomerization efficiency[17] and can be induced by aggregation.[46] Looking ahead, since excited-state inter- and intramolecular H-bonding dynamics are well-studied[47] and have a significant impact on solid-state optoelectronic properties,[48] additional excited-state studies with our systems will be important in the future.

Photopatterning Experiments. The inability to achieve quantitative photoisomerization with compounds **3a** and **1** in polystyrene may be due to smaller differences in absorption at the excitation wavelengths compared to chloroform, interactions with the polymer matrix, or the concentration of the chromophore within the polymer matrix. Even so, we demonstrated that photopatterning can be performed on polystyrene: **3a-*Z*** films with good color contrast between the *E*- and *Z*-enriched regions (Figure 13b2).

Much thicker polystyrene samples (∼2 mm) were loaded with 0.1 wt % (w/w) **3a-*Z*** to mimic a more application-relevant situation. Consecutive irradiation with 595 and 454 nm light facilitates reversible isomerization in the samples with excellent color contrast. Additional experiments are underway to explore how various polymer matrix environments influence the photostationary states of these compounds as well as studies investigating the difference in conductivity between *E* and *Z* isomers. Given their dissimilar aggregation behavior, we expect the electrical properties between *E* and *Z* films to be markedly different, as well.

The novel RCN-functionalized pyrrole photoswitches presented here were discovered to have an exciting

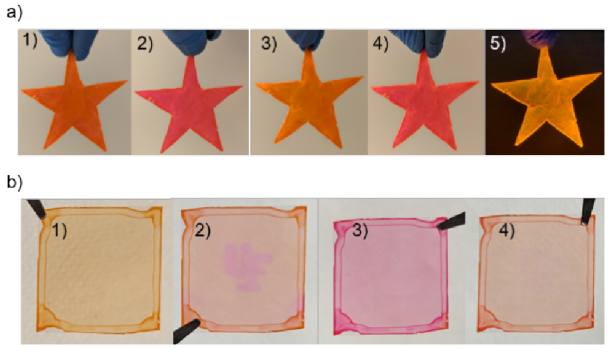

Figure 13. (a) Optical images of polystyrene films loaded with 0.1 wt % (w/w) **3a-*Z***: as-spun (1), after consecutive irradiations of 454 nm (2), 595 nm (3), 454 nm (4), and in a 365-nm UV light chamber (5). (b) Optical images of polystyrene films loaded with 1 wt % (w/w) **3a-*Z***: as-spun (1), after area-selective (2) or complete (3) 454 nm irradiation, and after 595 nm irradiation back to the *Z*-enriched PSS (4).

combination of unique properties such as quantitative photoswitching in solution, visible light photoswitching, excellent thermal stability, synthetic accessibility of pure *Z* and *E* states, reversible photoswitching in a polymer matrix, CIEE, photoisomerization in neat films, capability of vacuum deposition, and well-defined J- and H- aggregation for *E* and *Z* isomers. While some subset of these properties has been observed in previous photoswitching frameworks, we have not encountered photoswitching compounds with these same characteristics and see great potential for this new class of photoswitch. Further investigation is warranted to test whether these properties may be exploited fruitfully in practical applications.

CONCLUSIONS

To summarize, we have successfully developed six RCN-pyrrole conjugates and studied their photoisomerization behavior in solution and in the solid state. Both *Z* and *E* isomers were accessible from synthesis and could be separated using conventional silica gel column chromatography. Outstanding photoswitching performance was demonstrated by the target molecules, as reported by ^{1}H NMR and UV−vis spectroscopy. Quantitative photoisomerization was achieved for all cases with one model compound (**3a**) undergoing quantitative isomerization in both directions using light sources extending into the red part of the visible spectrum. This photoswitching bidirectionality presents RCN as a strong candidate for highly efficient molecular switches along with the well-known azobenzenes, HTIs, hydrazones, etc. Experimental and computational studies suggest intra- and intermolecular H-bonding interactions present in the *E* and *Z* isomers, respectively, which we hypothesize are central to their bistable nature. From detailed studies of the comparator molecules, H-bonding-capable pyrrole units improve the photoswitching capabilities of RCN-functionalized molecules more than benzene- or thiophene-functionalized molecules. UV−vis and PL spectra for neat films of compounds **1** and **3a** revealed remarkable differences in optical properties attributed to H-aggregation for *Z* isomers and J-aggregation for *E* isomers. The dramatic difference in transparency and PL intensity between the *E* and *Z* states facilitates a type of on−off switch that may prove to be advantageous for sensing applications. While photoisomerization in neat films was not shown to be

https://doi.org/10.1021/jacs.4c00983
J. Am. Chem. Soc. XXXX, XXX, XXX−XXX

bidirectional with our selected light sources, the extent of conversion was nearly quantitative in the case of **1**-*E* to **1**-*Z* and **3a**-*Z* to **3a**-*E* with mild heating. Moreover, reversible photoisomerization was successfully demonstrated for compounds **1** and **3a** in a photoinactive polystyrene matrix where two unique PSSs could be achieved using visible light sources including the Sun. Overall, this study presents the RCN-pyrrole conjugate as an excellent light-responsive unit worthy of investigation for photoswitching applications and as a test bed to better understand *E*/*Z* isomerization photophysics.

■ ASSOCIATED CONTENT

Supporting Information

The Supporting Information is available free of charge at https://pubs.acs.org/doi/10.1021/jacs.4c00983.

Synthesis schemes, written characterization data, ^{1}H NMR spectra, ^{13}C NMR spectra, 2D NMR characterization, NMR and UV−vis solution photoisomerization studies, variable temperature and concentration NMR studies, NMR thermal relaxation experiments, thin-film optical studies, polymer matrix photoswitching studies, computational details, and X-ray crystallography details. This material is available free of charge via the Internet at http://pubs.acs.org (PDF)

Accession Codes

CCDC 2325207, 2327100, and 2339365 contain the supplementary crystallographic data for this paper. These data can be obtained free of charge via www.ccdc.cam.ac.uk/data_request/cif, or by emailing data_request@ccdc.cam.ac.uk, or by contacting The Cambridge Crystallographic Data Centre, 12 Union Road, Cambridge CB2 1EZ, UK; fax: +44 1223 336 033.

■ AUTHOR INFORMATION

Corresponding Authors

Jiangeng Xue − *Department of Materials Science and Engineering, University of Florida, Gainesville, Florida 32611, United States*; Email: jxue@mse.ufl.edu

Ronald K. Castellano − *Department of Chemistry, University of Florida, Gainesville, Florida 32611, United States*; orcid.org/0000-0003-4322-9932; Email: castellano@chem.ufl.edu

Authors

Parag Das − *Department of Chemistry, University of Florida, Gainesville, Florida 32611, United States*

Nathan J. Grinalds − *Department of Materials Science and Engineering, University of Florida, Gainesville, Florida 32611, United States*

Ion Ghiviriga − *Department of Chemistry, University of Florida, Gainesville, Florida 32611, United States*; orcid.org/0000-0001-5812-5170

Khalil A. Abboud − *Department of Chemistry, University of Florida, Gainesville, Florida 32611, United States*

Łukasz Dobrzycki − *Department of Chemistry, University of Florida, Gainesville, Florida 32611, United States*

Complete contact information is available at: https://pubs.acs.org/10.1021/jacs.4c00983

Author Contributions

All authors have given approval to the final version of the manuscript.

Notes

The authors declare no competing financial interest.

■ ACKNOWLEDGMENTS

We are grateful to the National Science Foundation for funding this research (CHE-1904534 to RKC and JX; CHE-2203754 to RKC). We acknowledge University of Florida Research Computing for providing computational resources and support that have contributed to the research results reported in this publication (http://www.rc.ufl.edu). The mass spectrometric data were obtained by the UF Department of Chemistry Mass Spectrometry Research and Education Center supported, in part, by the National Institutes of Health (NIH S10 OD021758-01A1 and S10 OD030250-01A1). We would like to thank the UF Center for Nuclear Magnetic Resonance Spectroscopy for providing equipment and support that have contributed to these published results. The X-ray measurement was performed at the Center for X-ray Crystallography in the Department of Chemistry at the University of Florida. The NSF (CHE-1828064) and UF are greatly acknowledged for funding the X-ray diffractometer.

■ ABBREVIATIONS

RCN	dicyanorhodanine
OPV	organic photovoltaics
PSS	photostationary state
DFT	density functional theory
NMR	nuclear magnetic resonance
HTI	hemithioindigo
TLC	thin-layer chromatography

■ REFERENCES

(1) (a) Feringa, B. L.; Browne, W. R. *Molecular Switches*; John Wiley & Sons, 2011. (b) Feringa, B. L. *Molecular Photoswitches: Chemistry, Properties, and Applications, 2 Vol. Set*; John Wiley & Sons, 2022; pp 11083. (c) Feringa, B. L. The Art of Building Small: From Molecular Switches to Motors (Nobel Lecture). *Angew. Chem., Int. Ed.* **2017**, *56* (37), 11060−11078.

(2) (a) Beharry, A. A.; Woolley, G. A. Azobenzene photoswitches for biomolecules. *Chem. Soc. Rev.* **2011**, *40* (8), 4422−4437. (b) Mahimwalla, Z.; Yager, K. G.; Mamiya, J.-I.; Shishido, A.; Priimagi, A.; Barrett, C. J. Azobenzene photomechanics: Prospects and potential applications. *Polym. Bull.* **2012**, *69* (8), 967−1006. (c) Bandara, H. M. D.; Burdette, S. C. Photoisomerization in different classes of azobenzene. *Chem. Soc. Rev.* **2012**, *41* (5), 1809−1825.

(3) Waldeck, D. H. Photoisomerization dynamics of stilbenes. *Chem. Rev.* **1991**, *91* (3), 415−436.

(4) (a) Wiedbrauk, S.; Dube, H. Hemithioindigo—an emerging photoswitch. *Tetrahedron Lett.* **2015**, *56* (29), 4266−4274. (b) Wiedbrauk, S.; Maerz, B.; Samoylova, E.; Mayer, P.; Zinth, W.; Dube, H. Ingredients to TICT Formation in Donor Substituted Hemithioindigo. *J. Phys. Chem. Lett.* **2017**, *8* (7), 1585−1592. (c) Zitzmann, M.; Hampel, F.; Dube, H. A cross-conjugation approach for high-performance diaryl-hemithioindigo photoswitches. *Chem. Sci.* **2023**, *14* (21), 5734−5742.

(5) (a) Qian, H.; Pramanik, S.; Aprahamian, I. Photochromic Hydrazone Switches with Extremely Long Thermal Half-Lives. *J. Am. Chem. Soc.* **2017**, *139* (27), 9140−9143. (b) Shao, B.; Aprahamian, I. Hydrazones as New Molecular Tools. *Chem* **2020**, *6* (9), 2162−2173.

(6) (a) Klajn, R. Spiropyran-based dynamic materials. *Chem. Soc. Rev.* **2014**, *43* (1), 148−184. (b) Ali, A. A.; Kharbash, R.; Kim, Y. Chemo- and biosensing applications of spiropyran and its derivatives - A review. *Anal. Chim. Acta* **2020**, *1110*, 199−223.

(7) (a) Matsuda, K.; Irie, M. Diarylethene as a photoswitching unit. *J. Photochem. Photobiol., C* **2004**, *5* (2), 169−182. (b) Cheng, H.-B.;

https://doi.org/10.1021/jacs.4c00983
J. Am. Chem. Soc. XXXX, XXX, XXX−XXX

Zhang, S.; Bai, E.; Cao, X.; Wang, J.; Qi, J.; Liu, J.; Zhao, J.; Zhang, L.; Yoon, J. Future-Oriented Advanced Diarylethene Photoswitches: From Molecular Design to Spontaneous Assembly Systems. *Adv. Mater.* **2022**, *34* (16), 2108289. (c) Irie, M. *Diarylethene Molecular Photoswitches: concepts and Functionalities*; John Wiley & Sons, 2021.

(8) (a) Göstl, R.; Senf, A.; Hecht, S. Remote-controlling chemical reactions by light: Towards chemistry with high spatio-temporal resolution. *Chem. Soc. Rev.* **2014**, *43* (6), 1982−1996. (b) Zhang, J.; Zou, Q.; Tian, H. Photochromic Materials: More Than Meets The Eye. *Adv. Mater.* **2013**, *25* (3), 378−399.

(9) Brieke, C.; Rohrbach, F.; Gottschalk, A.; Mayer, G.; Heckel, A. Light-Controlled Tools. *Angew. Chem., Int. Ed.* **2012**, *51* (34), 8446−8476.

(10) (a) Kumar, P.; Gupta, D.; Grewal, S.; Srivastava, A.; Gaur, A. K.; Venkataramani, S. Multiple Azoarenes Based Systems − Photoswitching, Supramolecular Chemistry and Application Prospects. *Chem. Rec.* **2022**, *22* (11), No. e202200074. (b) Remón, P.; González, D.; Li, S.; Basílio, N.; Andréasson, J.; Pischel, U. Light-driven control of the composition of a supramolecular network. *ChemComm* **2019**, *55* (30), 4335−4338. (c) Ferreira, P.; Ventura, B.; Barbieri, A.; Da Silva, J. P.; Laia, C. A. T.; Parola, A. J.; Basílio, N. A Visible−Near-Infrared Light-Responsive Host−Guest Pair with Nanomolar Affinity in Water. *Chem. - Eur. J.* **2019**, *25* (14), 3477−3482. (d) Yao, X.; Li, T.; Wang, J.; Ma, X.; Tian, H. Recent Progress in Photoswitchable Supramolecular Self-Assembling Systems. *Adv. Opt. Mater.* **2016**, *4* (9), 1322−1349.

(11) (a) Russew, M.-M.; Hecht, S. Photoswitches: From Molecules to Materials. *Adv. Mater.* **2010**, *22* (31), 3348−3360. (b) Boelke, J.; Hecht, S. Designing Molecular Photoswitches for Soft Materials Applications. *Adv. Opt. Mater.* **2019**, *7* (16), 1900404. (c) Pianowski, Z. L. Recent Implementations of Molecular Photoswitches into Smart Materials and Biological Systems. *Chem. - Eur. J.* **2019**, *25* (20), 5128−5144. (d) Goulet-Hanssens, A.; Eisenreich, F.; Hecht, S. Enlightening Materials with Photoswitches. *Adv. Mater.* **2020**, *32* (20), 1905966.

(12) Ni, Y.; Li, X.; Hu, J.; Huang, S.; Yu, H. Supramolecular liquid-crystalline polymer organogel: Fabrication, multiresponsiveness, and holographic switching properties. *Chem. Mater.* **2019**, *31* (9), 3388−3394.

(13) (a) Abendroth, J. M.; Bushuyev, O. S.; Weiss, P. S.; Barrett, C. J. Controlling Motion at the Nanoscale: Rise of the Molecular Machines. *ACS Nano* **2015**, *9* (8), 7746−7768. (b) Kassem, S.; van Leeuwen, T.; Lubbe, A. S.; Wilson, M. R.; Feringa, B. L.; Leigh, D. A. Artificial molecular motors. *Chem. Soc. Rev.* **2017**, *46* (9), 2592−2621. (c) Roke, D.; Sen, M.; Danowski, W.; Wezenberg, S. J.; Feringa, B. L. Visible-Light-Driven Tunable Molecular Motors Based on Oxindole. *J. Am. Chem. Soc.* **2019**, *141* (18), 7622−7627. (d) Uhl, E.; Mayer, P.; Dube, H. Active and Unidirectional Acceleration of Biaryl Rotation by a Molecular Motor. *Angew. Chem., Int. Ed.* **2020**, *59* (14), 5730−5737.

(14) (a) Mukherjee, A.; Seyfried, M. D.; Ravoo, B. J. Azoheteroarene and Diazocine Molecular Photoswitches: Self-Assembly, Responsive Materials and Photopharmacology. *Angew. Chem., Int. Ed.* **2023**, *62*, No. e202304437. (b) Kobauri, P.; Dekker, F. J.; Szymanski, W.; Feringa, B. L. Rational Design in Photopharmacology with Molecular Photoswitches. *Angew. Chem., Int. Ed.* **2023**, *62* (30), No. e202300681. (c) Broichhagen, J.; Frank, J. A.; Trauner, D. A Roadmap to Success in Photopharmacology. *Acc. Chem. Res.* **2015**, *48* (7), 1947−1960.

(15) (a) Rapp, T. L.; DeForest, C. A. Targeting drug delivery with light: A highly focused approach. *Adv. Drug Delivery Rev.* **2021**, *171*, 94−107. (b) Fitzmaurice, O.; Bartkowski, M.; Giordani, S. Molecular Switches—Tools for Imparting Control in Drug Delivery Systems. *Front. Chem.* **2022**, *10* (10), 859450.

(16) (a) Bléger, D.; Hecht, S. Visible-Light-Activated Molecular Switches. *Angew. Chem., Int. Ed.* **2015**, *54* (39), 11338−11349. (b) Zhang, Z.; Wang, W.; O'Hagan, M.; Dai, J.; Zhang, J.; Tian, H. Stepping Out of the Blue: From Visible to Near-IR Triggered Photoswitches. *Angew. Chem., Int. Ed.* **2022**, *61* (31), No. e202205758. (c) Leistner, A.-L.; Pianowski, Z. L. Smart Photochromic Materials Triggered with Visible Light. *Eur. J. Org. Chem.* **2022**, *2022* (19), No. e202101271.

(17) Krell-Jørgensen, M.; Zulfikri, H.; Bonnevie, M. G.; Bro, F. S.; Dohn, A. O.; Laraia, L. Redshifted and thermally bistable one-way quantitative hemithioindigo-derived photoswitches enabled by isomer-specific excited state intramolecular proton transfer. *ChemCommun* **2023**, *59* (5), 563−566.

(18) Sheng, J.; Danowski, W.; Crespi, S.; Guinart, A.; Chen, X.; Stähler, C.; Feringa, B. L. Designing p-type bi-stable overcrowded alkene-based chiroptical photoswitches. *Chem. Sci.* **2023**, *14* (16), 4328−4336.

(19) (a) Tanaka, K.; Taguchi, K.; Iwata, S.; Irie, T. Novel photochromic behavior of benzoylhemithioindigo based on photodimerization. *Chem. Lett.* **2004**, *33* (7), 848−849. (b) Tanaka, k.; Kohayakawa, k.; Irie, T.; Iwata, S.; Taguchi, K. Novel photoinduced cyclization of pentafluorophenylhemithioindigo. *J. Fluor. Chem.* **2007**, *128* (10), 1094−1097.

(20) Weston, C. E.; Richardson, R. D.; Haycock, P. R.; White, A. J. P.; Fuchter, M. J. Arylazopyrazoles: Azoheteroarene Photoswitches Offering Quantitative Isomerization and Long Thermal Half-Lives. *J. Am. Chem. Soc.* **2014**, *136* (34), 11878−11881.

(21) (a) Villarón, D.; Wezenberg, S. J. Stiff-Stilbene Photoswitches: From Fundamental Studies to Emergent Applications. *Angew. Chem., Int. Ed.* **2020**, *59* (32), 13192−13202. (b) Volarić, J.; Szymanski, W.; Simeth, N. A.; Feringa, B. L. Molecular photoswitches in aqueous environments. *Chem. Soc. Rev.* **2021**, *50* (22), 12377−12449.

(22) Zweig, J. E.; Newhouse, T. R. Isomer-Specific Hydrogen Bonding as a Design Principle for Bidirectionally Quantitative and Redshifted Hemithioindigo Photoswitches. *J. Am. Chem. Soc.* **2017**, *139* (32), 10956−10959.

(23) Josef, V.; Hampel, F.; Dube, H. Heterocyclic Hemithioindigos: Highly Advantageous Properties as Molecular Photoswitches. *Angew. Chem., Int. Ed.* **2022**, *61* (43), No. e202210855.

(24) Köttner, L.; Wolff, F.; Mayer, P.; Zanin, E.; Dube, H. Rhodanine-Based Chromophores: Fast Access to Capable Photoswitches and Application in Light-Induced Apoptosis. *J. Am. Chem. Soc.* **2024**, *146* (3), 1894−1903.

(25) (a) Insuasty, A.; Ortiz, A.; Tigreros, A.; Solarte, E.; Insuasty, B.; Martín, N. 2-(1,1-dicyanomethylene)rhodanine: A novel, efficient electron acceptor. *Dyes Pigm.* **2011**, *88* (3), 385−390. (b) Kan, B.; Li, M.; Zhang, Q.; Liu, F.; Wan, X.; Wang, Y.; Ni, W.; Long, G.; Yang, X.; Feng, H.; Zuo, Y.; Zhang, M.; Huang, F.; Cao, Y.; Russell, T. P.; Chen, Y. A Series of Simple Oligomer-like Small Molecules Based on Oligothiophenes for Solution-Processed Solar Cells with High Efficiency. *J. Am. Chem. Soc.* **2015**, *137* (11), 3886−3893.

(26) (a) Fan, Q.; Li, M.; Yang, P.; Liu, Y.; Xiao, M.; Wang, X.; Tan, H.; Wang, Y.; Yang, R.; Zhu, W. Acceptor-donor-acceptor small molecules containing benzo[1,2-*b*: 4,5-*b*′]dithiophene and rhodanine units for solution processed organic solar cells. *Dyes Pigm.* **2015**, *116*, 13−19. (b) Privado, M.; de la Cruz, P.; Gupta, G.; Singhal, R.; Sharma, G. D.; Langa, F. Highly efficient ternary polymer solar cell with two non-fullerene acceptors. *Sol. Energy* **2020**, *199*, 530−537. (c) Liu, F.; Zhou, L.; Liu, W.; Zhou, Z.; Yue, Q.; Zheng, W.; Sun, R.; Liu, W.; Xu, S.; Fan, H.; Feng, L.; Yi, Y.; Zhang, W.; Zhu, X. Organic Solar Cells with 18% Efficiency Enabled by an Alloy Acceptor: A Two-in-One Strategy. *Adv. Mater.* **2021**, *33* (27), 2100830. (d) Duan, T.; Chen, Q.; Yang, Q.; Hu, D.; Cai, G.; Lu, X.; Lv, J.; Song, H.; Zhong, C.; Liu, F.; Yu, D.; Lu, S. Simple thiazole-centered oligothiophene donor enables 15.4% efficiency all small molecule organic solar cells. *J. Mater. Chem. A* **2022**, *10* (6), 3009−3017.

(27) Kornman, C. T.; Li, L.; Weldeab, A. O.; Ghiviriga, I.; Abboud, K. A.; Castellano, R. K. Photoisomerization of dicyanorhodanine-functionalized thiophenes. *Chem. Sci.* **2020**, *11* (37), 10190−10197.

(28) Camero, D. M.; Grinalds, N. J.; Kornman, C. T.; Barba, S.; Li, L.; Weldeab, A. O.; Castellano, R. K.; Xue, J. Thin-Film Morphology and Optical Properties of Photoisomerizable Donor−Acceptor Oligothiophenes. *ACS Appl. Mater. Interfaces* **2023**, *15* (21), 25134−25147.

https://doi.org/10.1021/jacs.4c00983
J. Am. Chem. Soc. XXXX, XXX, XXX−XXX

(29) Scalmani, G.; Frisch, M. J.; Mennucci, B.; Tomasi, J.; Cammi, R.; Barone, V. Geometries and properties of excited states in the gas phase and in solution: Theory and application of a time-dependent density functional theory polarizable continuum model. *J. Chem. Phys.* **2006**, *124* (9), 094107.
(30) Wang, X.; Xu, B.; Tian, W. Solid-State Luminescent Molecular Photoswitches. *Acc. Mater. Res.* **2023**, *4* (4), 311−322.
(31) Zweig, J. E.; Ko, T. A.; Huang, J.; Newhouse, T. R. Effects of π-extension on pyrrole hemithioindigo photoswitches. *Tetrahedron* **2019**, *75* (34), 130466.
(32) (a) Ji, G.; Wang, N.; Yin, X.; Chen, P. Substituent Effect Induces Emission Modulation of Stilbene Photoswitches by Spatial Tuning of the N/B Electronic Constraints. *Org. Lett.* **2020**, *22* (15), 5758−5762. (b) Li, Z.; Liu, Y.; Yang, X.-G.; Gao, X.; Zhang, Y.; Zhang, H.; Kang, G.; Wang, M.; Guo, H. Cyanostilbene-functionalized dithienylethenes with aggregation-induced emission for photoswitching behavior in multi-media. *J. Lumin.* **2022**, *250*, 119061.
(33) Das, P.; Kornman, C. T.; Ghiviriga, I.; Abboud, K. A.; Castellano, R. K. Enlightening the Well-Controlled Photochemical Behavior of 1,1-Dicyanomethylene-3-Indanone-Functionalized π-Conjugated Molecules. *Chem. Mater.* **2023**, *35* (19), 8122−8134.
(34) Sigalov, M.; Shainyan, B.; Chipanina, N.; Oznobikhina, L.; Strashnikova, N.; Sterkhova, I. Molecular Structure and Photoinduced Intramolecular Hydrogen Bonding in 2-Pyrrolylmethylidene Cycloalkanones. *J. Org. Chem.* **2015**, *80* (21), 10521−10535.
(35) Sigalov, M. V.; Shainyan, B. A.; Chipanina, N. N.; Oznobikhina, L. P.; Kuzmin, A. V. *E*→*Z* photoinduced isomerization and hydrogen bonding in the peri-acetamido substituted (1H-pyrrol-2-ylmethylene)benzocycloalkanones. *Tetrahedron* **2020**, *76* (21), 131202.
(36) Sigalov, M. V.; Shainyan, B. A.; Sterkhova, I. V. Photoinduced Intramolecular Bifurcate Hydrogen Bond: Unusual Mutual Influence of the Components. *J. Org. Chem.* **2017**, *82* (17), 9075−9086.
(37) Kohl, F.; Gerwien, A.; Hampel, F.; Mayer, P.; Dube, H. Hemithioindigo-Based Trioxobicyclononadiene: 3D Multiswitching of Electronic and Geometric Properties. *J. Am. Chem. Soc.* **2022**, *144* (7), 2847−2852.
(38) (a) Hu, H.; Liu, B.; Li, M.; Zheng, Z.; Zhu, W.-H. Quadri-Dimensional Manipulable Laser with an Intrinsic Chiral Photoswitch. *Adv. Mater.* **2022**, *34* (15), 2110170. (b) Naren, G.; Hsu, C.-W.; Li, S.; Morimoto, M.; Tang, S.; Hernando, J.; Guirado, G.; Irie, M.; Raymo, F. M.; Sundén, H.; Andreasson, J. An all-photonic full color RGB system based on molecular photoswitches. *Nat. Commun.* **2019**, *10* (1), 3996. (c) Marazzi, M.; García-Iriepa, C.; Benitez-Martin, C.; Najera, F.; Monari, A.; Sampedro, D. *E*/*Z* Molecular Photoswitches Activated by Two-Photon Absorption: Comparison between Different Families. *Molecules* **2021**, *26* (23), 7379. (d) Wu, Y.; Guo, Z.; Zhu, W.-H.; Wan, W.; Zhang, J.; Li, W.; Li, X.; Tian, H.; Li, A. D. Q. Photoswitching between black and colourless spectra exhibits resettable spatiotemporal logic. *Mater. Horiz.* **2016**, *3* (2), 124−129. (e) Ishiguro, Y.; Hayakawa, R.; Chikyow, T.; Wakayama, Y. Optical switching of carrier transport in polymeric transistors with photochromic spiropyran molecules. *J. Mater. Chem. C* **2013**, *1* (17), 3012−3016.
(39) (a) Kasha, M.; Rawls, H. R.; El-Bayoumi, M.A. The exciton model in molecular spectroscopy. *J. Pure Appl. Chem.* **1965**, *11*, 371−392. (b) Spano, F. C. The Spectral Signatures of Frenkel Polarons in H- and J-Aggregates. *Acc. Chem. Res.* **2010**, *43* (3), 429−439.
(40) (a) Hestand, N. J.; Spano, F. C. Molecular Aggregate Photophysics beyond the Kasha Model: Novel Design Principles for Organic Materials. *Acc. Chem. Res.* **2017**, *50* (2), 341−350. (b) Bricks, J. L.; Slominskii, Y. L.; Panas, I. D.; Demchenko, A. P. Fluorescent J-aggregates of cyanine dyes: Basic research and applications review. *Methods Appl. Fluoresc.* **2018**, *6* (1), 012001.
(41) Schötz, K.; Panzer, F.; Sommer, M.; Bässler, H.; Köhler, A. A spectroscopic assessment of static and dynamic disorder in a film of a polythiophene with a planarized backbone. *Mater. Horiz.* **2023**, *10* (12), 5538−5546.
(42) Yoshii, R.; Hirose, A.; Tanaka, K.; Chujo, Y. Boron Diiminate with Aggregation-Induced Emission and Crystallization-Induced Emission-Enhancement Characteristics. *Chem. - Eur. J.* **2014**, *20* (27), 8320−8324.
(43) (a) Gopikrishna, P.; Iyer, P. K. Monosubstituted Dibenzofulvene-Based Luminogens: Aggregation-Induced Emission Enhancement and Dual-State Emission. *J. Phys. Chem. C* **2016**, *120* (46), 26556−26568. (b) Choi, S.; Bouffard, J.; Kim, Y. Aggregation-induced emission enhancement of a meso-trifluoromethyl BODIPY via J-aggregation. *Chem. Sci.* **2014**, *5* (2), 751−755. (c) Feng, X.; Tong, B.; Shen, J.; Shi, J.; Han, T.; Chen, L.; Zhi, J.; Lu, P.; Ma, Y.; Dong, Y. Aggregation-Induced Emission Enhancement of Aryl-Substituted Pyrrole Derivatives. *J. Phys. Chem. B* **2010**, *114* (50), 16731−16736.
(44) Chang, X.; Qarai, M. B.; Spano, F. C. HJ-aggregates of donor−acceptor−donor oligomers and polymers. *J. Chem. Phys.* **2021**, *155* (3), 034905. (b) Würthner, F.; Kaiser, T. E.; Saha-Möller, C. R. J-Aggregates: From Serendipitous Discovery to Supramolecular Engineering of Functional Dye Materials. *Angew. Chem., Int. Ed.* **2011**, *50* (15), 3376−3410. (c) Yamagata, H.; Pochas, C. M.; Spano, F. C. Designing J- and H-Aggregates through Wave Function Overlap Engineering: Applications to Poly(3-hexylthiophene). *J. Phys. Chem. B* **2012**, *116* (49), 14494−14503.
(45) Joshi, H. C.; Antonov, L. Excited-State Intramolecular Proton Transfer: A Short Introductory Review. *Molecules* **2021**, *26* (5), 1475.
(46) Zhao, J.; Dong, H.; Yang, H.; Zheng, Y. Aggregation Promotes Excited-State Intramolecular Proton Transfer for Benzothiazole-Substituted Tetraphenylethylene Compound. *ACS Appl. Bio Mater.* **2019**, *2* (11), 5182−5189.
(47) Zhao, G.-J.; Han, K.-L. Hydrogen Bonding in the Electronic Excited State. *Acc. Chem. Res.* **2012**, *45* (3), 404−413.
(48) (a) Liu, Y.; Tao, X.; Wang, F.; Shi, J.; Sun, J.; Yu, W.; Ren, Y.; Zou, D.; Jiang, M. Intermolecular Hydrogen Bonds Induce Highly Emissive Excimers: Enhancement of Solid-State Luminescence. *J. Phys. Chem. C* **2007**, *111* (17), 6544−6549. (b) Dommett, M.; Rivera, M.; Crespo-Otero, R. How Inter- and Intramolecular Processes Dictate Aggregation-Induced Emission in Crystals Undergoing Excited-State Proton Transfer. *J. Phys. Chem. Lett.* **2017**, *8* (24), 6148−6153.

https://doi.org/10.1021/jacs.4c00983
J. Am. Chem. Soc. XXXX, XXX, XXX−XXX